

ac Josephson effect in superconducting d -wave junctions

Magnus Hurd*, Tomas Löfwander, Göran Johansson, and Göran Wendin
*Department of Microelectronics and Nanoscience, School of Physics and Engineering Physics,
 Chalmers University of Technology and Göteborg University,
 S-412 96 Göteborg, Sweden*

(February 27, 2018)

We study theoretically the ac Josephson effect in superconducting planar d -wave junctions. The insulating barrier assumed to be present between the two superconductors may have arbitrary strength. Many properties of this system depend on the orientation of the d -wave superconductor: we calculate the ac components of the Josephson current. In some arrangements there is substantial negative differential conductance due to the presence of mid-gap states. We study how robust these features are to finite temperature and also comment on how the calculated current-voltage curves compare with experiments. For some other configurations (for small barrier strength) we find zero-bias conductance peaks due to multiple Andreev reflections through midgap states. Moreover, the odd ac components are strongly suppressed and even absent in some arrangements. This absence will lead to a doubling of the Josephson frequency. All these features are due to the d -wave order parameter changing sign when rotated 90° . Recently, there have been several theoretical reports on parallel current in the d -wave case for both the stationary Josephson junction and for the normal metal-superconductor junction. Also in our case there may appear current density parallel to the junction, and we present a few examples when this takes place. Finally, we give a fairly complete account of the method used and also discuss how numerical calculations should be performed in order to produce current-voltage curves.

PACS numbers: 74.50.+r, 74.25, 74.20.-z

I. INTRODUCTION

There are now strong reasons to believe that many of the high- T_c superconductors (HTS) exhibit a superconducting order parameter which has mainly (or completely) $d_{x^2-y^2}$ -wave (d -wave) symmetry.^{1,2} The exact structure of the order parameter depends on the material. For instance, due to the orthorhombic character of $\text{YBa}_2\text{Cu}_3\text{O}_{7-\delta}$ (YBCO) an s -wave component of the order parameter is induced.³ This is not the case for tetragonal systems like $\text{Tl}_2\text{Ba}_2\text{CuO}_{6+\delta}$, where a pure $d_{x^2-y^2}$ -wave symmetry has been established.⁴ At any rate, the presence of a substantial component of d -wave symmetry in the high- T_c superconductors cannot be ignored.

This paper sets out to explore theoretically the implications of d -wave symmetry for the ac Josephson effect in high- T_c superconductors.

To have the ac Josephson effect, two superconductors must be present on both sides of a normal (or insulating) region as shown in Fig. 1. For an anisotropic superconductor the order parameter $\Delta(\theta)$ depends on the angle θ of incidence of the quasiparticle approaching the junction region. In the case of pure d -wave symmetry we have $\Delta(\theta) = \Delta_0 \cos[2(\theta - \alpha)]$, where α is the orientation of the d -wave order parameter with respect to the insulator. We will in this paper use the notation d_α for d -wave superconductor with orientation α . For the isotropic s -wave case, $\Delta(\theta) = \Delta_s$. Another competing candidate for the order parameter of HTS has been the anisotropic s -wave order parameter: $\Delta(\theta) = \Delta_0 \cos^4[2(\theta - \alpha)] + \Delta_1$; today, however, it does not seem to be on the short list of possible HTS order parameters any longer.²⁻⁴

The strength of the insulating barrier shown in Fig. 1 may vary in our treatment. This makes it possible to treat all superconductor-superconductor junctions from the ballistic (fully transparent) superconductor-normal metal-superconductor (SNS) junction to the superconductor-insulator-superconductor (SIS) tunnel junction. To describe superconductor-superconductor junctions in general we use the notation $S_1|S_2$ where $S_{1(2)}$ is the superconductor on the left (right) side of the interface $|$. The interface is a barrier of arbitrary strength.

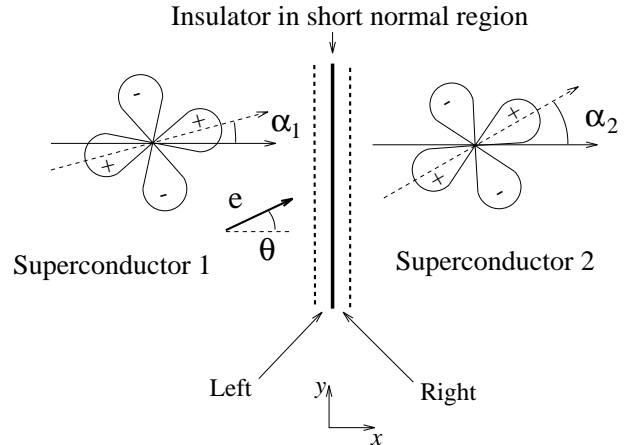


FIG. 1. Layout of the junction. The orientations of the two d -wave superconductors are described by the angles α_1 and α_2 . An electron-like quasiparticle is incident on the junction at an angle θ . Short normal regions are introduced between the barrier and the superconductors. The strength of the barrier can be tuned from the ballistic to the insulating case.

The ac Josephson effect, from a general point of view,

means that for an S|S junction a time independent bias voltage V results in a time dependent current. The non-stationary current perpendicular to the junction (the x -direction; see Fig. 1) can be decomposed into frequency components

$$I_x(V, t) = \sum_m I_{x,m}(V) e^{im\omega_J t}, \quad (1)$$

where m is an integer. The Josephson frequency $\omega_J = 2eV/\hbar$ corresponds to the energy gained by a Cooper pair when passing through the junction region. Since the relation $I_{x,-m}(V) = I_{x,m}^*(V)$ holds, the current is real.

An order parameter with $d_{x^2-y^2}$ -wave symmetry changes sign when rotated 90° . This feature has been shown to have several implications on transport properties of $d_{x^2-y^2}$ -wave superconductors, some of which have been confirmed in experiments: cancellation effects as to the dc Josephson current¹⁻⁴ and the presence of zero-bias conductance peaks (ZBCP) in various structures of HTS junctions.⁵⁻¹⁰ Since in this paper the focus is on the ac Josephson effect we will (among other things) discuss issues related to ZBCP.

The ZBCP arises due to the presence of zero-energy bound states, so-called midgap states (MGS), at surfaces/interfaces of $d_{x^2-y^2}$ -wave superconductors.¹¹ The reason MGS appear is an interplay between normal scattering (at the surface/interface) and the fact that the d -wave order parameter changes sign at some regions in momentum space. Since in the d -wave case the order parameter depends on momentum (or in other words angle θ), a quasiparticle will in general sense a different order parameter before and after scattering (normal scattering changes the momentum). When there is a sign difference of the order parameter before and after scattering a zero-energy bound state appears (MGS).¹¹ These localized zero-energy states open up additional channels for current flow, leading to peaks in the conductance. Calculations of the current-voltage ($I - V$) curves for the normal metal-superconductor (NS) junction¹² confirmed the picture brought forward in Ref. 11. MGS are infinitely sharp when the transmission of the strength of the barrier is infinitely high. When the strength of the barrier decreases the MGS broaden.

In addition, there are some other features related to the ac Josephson effect involving d -wave superconductors that have not yet (to our knowledge) been experimentally established, such as negative differential conductance¹³⁻¹⁶ and cancellation of the odd ac components, doubling the Josephson frequency,¹⁷ although there are experiments discussing related features.^{7,18} Negative differential conductance is a result of resonant conduction through MGS.¹³ Moreover, we will in this paper show an example of ZBCP for the case when there are MGS on both sides of the barrier (possible only when there are d -wave superconductors on both sides of the barrier). We note that for the cases we discuss ZBCP appear for relatively small values of barrier strength. The

geometry used in these calculations correspond to experiments just recently performed.^{9,10}

Cancellation of the odd ac components is explained as follows (see Fig. 2). The keypoint is that the total current is a sum of contributions, associated with different angles θ . In the case of two d -wave superconductors with orientation angles $\alpha_1 = 0$ and $\alpha_2 = \pi/4$ respectively, quasiparticles incident at angle $-\theta$ experience a different sign of the gap Δ_2 compared to quasiparticles incident at θ . This sign difference (which corresponds to a phase difference of π) enters the expression of ac components as $e^{im\pi} = (-1)^m$, where m is the index of the ac component in Eq. (1). This means that for even (odd) m , positive and negative angles add up (cancel out).¹⁷ We note that the doubling of the Josephson frequency is completely in line with the change of the current-phase relationship in stationary Josephson junctions from being 2π -periodic to being π -periodic in some arrangements.¹⁹⁻²²

Moreover, there appears in voltage-biased junctions of d -wave superconductors a possibility to have current flow parallel to the junction. This is not necessarily related to the ac Josephson effect but could appear in NS junctions as well.¹⁷

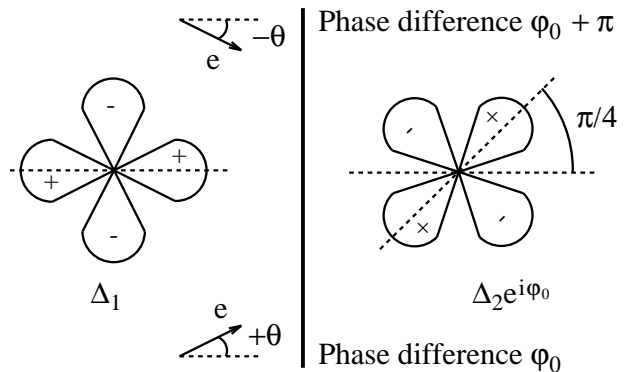


FIG. 2. Symmetry argument for the cancellation of the odd ac components for the specific orientation $d_0|d_{\pi/4}$. Considering injection of electron-like quasiparticles at angles $\pm\theta$, the gap in the left superconductor will be the same, while there will be a sign difference in the right superconductor. In the above figure, the negative sign appears at $-\theta$ and can be thought of as an extra phase π for this injection angle. The current contributions from $\pm\theta$ are equal in magnitude but have different signs for the odd components, because of the extra phase π , and will therefore cancel.

Recently, there has been a discussion concerning the appearance of superconducting states breaking time-reversal symmetry, especially at inhomogeneities (like surfaces/interfaces) in d -wave superconductors. These states have been theoretically predicted to have an order parameter of the form $d + is$, where the is -part is induced by the inhomogeneity and only present close to the inhomogeneity. The is -wave part of the order parameter has vital physical importance: the $d + is$ combination explicitly breaks time-reversal symmetry, and peculiar surface/interface currents appear with the existence of the

is part. One example of this phenomenon is twin boundaries of YBCO, whose order parameter is of the form $d \pm s$ (a real combination). The twin boundary divides the superconductor into two parts with different signs in front of the *s*-part. To match the two sides the most favorable way (from a Ginzburg-Landau theoretical point of view), close to the boundary a complex order parameter appears in order to avoid a discontinuous change in the phase between the *s*- and *d*-part of the order parameter.²³ This result has also been found within a Green's function formalism²⁴ and by solving the Bogoliubov-de Gennes equation.²⁵ Another example is the surface of a *d*-wave superconductor, where the surface lowers the symmetry in such a way that a combination of the subdominant *s* and the dominant *d* order parameters are now allowed at temperatures below a certain temperature defined by various properties, giving rise to a $d+is$ surface state with associated time-reversal symmetry breaking currents parallel to the surface.^{6,26-28} These surface states are doubly degenerate, corresponding to two opposite current directions. A third example (and most closely related to the case studied in this paper) is the junction between an *s*-wave superconductor and a $d_{x^2-y^2}$ -wave superconductor rotated 45° ,²⁹ where a combination of *s*- and *d*-waves coexists close to the junction area. Again the phase difference of the energetically stable phase is such that a $d \pm is$ order parameter appears, also this time doubly degenerate corresponding to phase differences of $\pm\pi/2$ between the *s*- and *d*-wave side. The same effect has theoretically been found in junctions between two $d_{x^2-y^2}$ superconductors where one of the superconductors is rotated by 45° .³⁰

All the examples discussed above concern the stationary state. This is definitely different from our case with a voltage present between the two sides of the junction.^{13,17} In fact, when the junction is voltage-biased it does not care about the ground state phase difference between the two sides. Rather, all possible phases are taking part in an averaging procedure. Therefore, it is not surprising that the case discussed in Ref. 29 (the third example in the previous paragraph) does not produce parallel current density for the zero-frequency ac component in the voltage-biased case, since the two degenerate states (corresponding to two opposite current directions) are now averaged to produce a zero net dc current density. In Fig. 3 we show the mechanism in the voltage biased case for the net current density parallel to the interface between the two sides. The bottomline is that a $d_{x^2-y^2}$ -wave order parameter with orientation angle $\alpha \neq 0$ treats quasiparticles associated with positive injection angles differently than quasiparticles associated with negative injection angles, leading to an imbalance between current contributions associated with positive and negative injection angles.

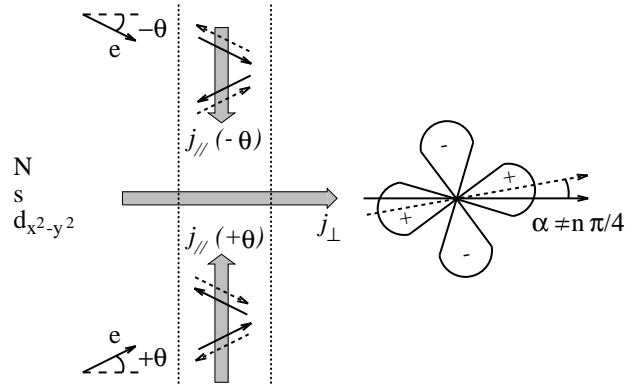


FIG. 3. This picture shows how the parallel (*y*-direction) current appears as a consequence of the asymmetry of the *d*-wave order parameter. On the left side we have a normal, an *s*-wave or a *d*-wave structure; on the right side we have a *d*-wave superconductor with $\alpha \neq n\pi/4$, where n is an integer. Quasiparticles incident on the right side (from the left) in general experience a different gap depending on angle of incidence θ . Since current contributions (among other things) depend on the gap this means that the parallel current contribution corresponding to θ does not necessarily cancel the one corresponding to $-\theta$. The solid and dashed lines illustrate electrons and holes propagating in both directions.

Therefore, in this paper we consider the ac Josephson effect and focus on three main issues: first, current-voltage curves of *d*-wave $S_1|S_2$ junctions; second, the disappearance of the odd ac components; third, the current density parallel to the junction direction. Moreover, we give a fairly complete account of the methods used.^{13,17} Especially, we elaborate on how various ways of writing down current formulas relate to each other.

In the case of *s*-wave superconductivity Eq. (1) has been studied for a long time. In the tunneling limit (low transmission of the insulating barrier) detailed calculations³¹⁻³³ showed excellent agreement with experimental results for the conventional *s*-wave superconductors. These calculations used the tunneling hamiltonian method. Due to the huge success of the tunneling calculations less attention was paid to the non-tunneling case.

The work by Blonder, Tinkham, and Klapwijk proved that with fairly simple methods it was possible to produce current-voltage curves of NS junctions for any barrier strength.³⁴ Later, another line of research focused on introducing the concept of mesoscopics into superconductivity.³⁵⁻³⁹ Both the dc Josephson effect^{35,36} and the ac Josephson effect³⁷⁻³⁹ were studied, again without the tunneling-limit restriction.

The main tool in many of these papers dealing with the case of arbitrary transmission has been the Bogoliubov-de Gennes (BdG) equation.^{34-36,38,39} The time-dependent BdG equation together with a formula for the current gives a complete description of the current in both the stationary and non-stationary case. In this paper we use a generalization^{13,17} of the methods worked out for the *s*-wave case.³⁸⁻⁴¹

When an electron with subgap energy from a normal

region approaches the superconductor, there seems to be no way of transmitting electric charge into the superconductor: there are no propagating states of the superconductor in the subgap region. This becomes evident when solving the Bogoliubov-de Gennes (BdG) equation resulting in decaying wave functions when solving for subgap energies.^{34,42}

However, there is one important physical process making transmission of electric charge possible also for subgap incidence: Andreev reflection (AR).^{34,43} In this process an electron (from a normal region) with subgap energy incident on a superconductor is reflected as a hole moving in the opposite direction to the original electron. This event does obviously not in itself conserve particles. Therefore, a Cooper pair of electrons is injected into the superconductor. When two superconductors embrace the normal region, forming an SNS junction, the hole will finally hit the other superconductor and again Andreev reflects, this time as an electron. These AR's will continue back and forth in the normal region. Since the voltage drop is over the normal region, the electrons and holes gain the energy eV every time they pass the normal region (see Fig. 4). These repeated reflections are usually named multiple Andreev reflections (MAR). The reflections are perfect inside the gap but decrease in strength when the magnitude of the excitation energy is increased away from the gap region.

For each round trip two AR's transform the original electron into an electron at an energy $2eV$ higher than from the start. This means that the wave functions contain parts (sidebands) separated by multiples of $2eV$ from each other, leading to an ac current with a frequency of $2eV/\hbar$ as seen in Eq. (1).

We think Fig. 4 is a key figure in order to illustrate the underlying physical mechanism of the phenomenon discussed in this paper (the ac Josephson effect): it makes clear the meaning of Eq. (1). There are two scattering events of our problem: first, normal scattering at the barrier described by a transmission amplitude; second, AR at the NS interfaces described by an AR amplitude. Therefore, Eq. (1) can be thought of as an expansion in transmission amplitude (through the barrier) and AR amplitude. Higher orders of the wave function corresponding to sidebands visualized in Fig. 4 contain higher orders of transmission through the barrier and higher orders of AR.

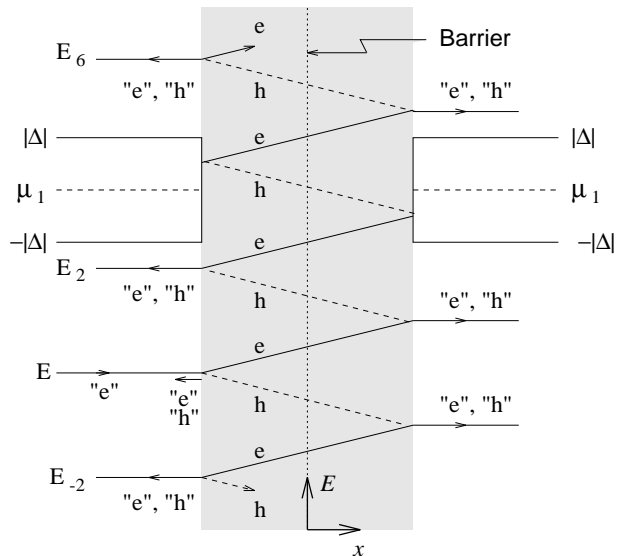


FIG. 4. The scattering state originating from an electron-like quasiparticle incident at energy E . There are electrons and holes propagating in both directions (no arrows included in the figure) in the normal region at energies $E_n = E + neV$, where n is an integer and V is the voltage over the junction. The shaded area is the junction region where the voltage drop occurs.

The present paper is organized in the following way. In Section II we outline the model, which is used in Section III to calculate the various ac components of the current. We present the results in Section IV, and conclude with a summary in Section V. We feel that an important part of our paper is given in the appendices: in Appendix A the time-dependent BdG equation is solved, and we also give some numerical advice on how to calculate the current; in Appendix B we compare how various current formulas previously used in the literature relate to each other; in Appendix C we point out a couple of symmetry relations that are relevant to our problem; finally, in Appendix D we write down a pair of analytical expressions describing the ballistic case.

II. THE MODEL

To mathematically describe the voltage-biased $S_1|S_2$ system shown in Fig. 1 we have made a number of assumptions, some of them pertaining to the superconducting parts of the system and some of them pertaining to the normal part of the system. In the following we detail these assumptions.

Starting with the normal part (the junction) in between the superconductors, we assume a planar structure with translational invariance in the y -direction. The planar geometry is a necessary condition for MGS to exist, contrary to the case of point contacts⁴⁴ where no MGS are around. Moreover, we neglect in our treatment any influence from interface roughness. In the normal region we only take into account scattering due to

the barrier, which is modeled as a one-particle potential $V(x) = H\delta(x)$. The δ -function form of $V(x)$ results in a reflection amplitude $r(\theta) = Z/(i\cos\theta - Z)$ and a transmission amplitude $t(\theta) = i\cos\theta/(i\cos\theta - Z)$, where Z is defined as $Z = 2mH/\hbar^2$.⁴⁵ The parameter Z describes the strength of the barrier: $Z = 0$ corresponds to no scattering at all (ballistic case); $Z = \infty$ corresponds to the case when the two sides of the junction are uncoupled (no x -current in this case); a high value of Z corresponds to the tunneling case.

Next we consider the superconducting parts. In our calculation self-consistency is not fulfilled. In the literature there is work that has included self-consistency in the tunneling limit showing that non-zero energy states appear along with MGS.^{14,15} In our work we neglect these effects; on the other hand, we allow the barrier strength Z of the barrier to have any value.

Therefore, we assume that the superconducting order parameter of the structure in Fig. 1 is

$$\Delta = \begin{cases} \Delta_1(\theta), & x < 0 \\ \Delta_2(\theta)e^{i\phi_0}, & x > 0. \end{cases} \quad (2)$$

Since the overall phase is unimportant we can here choose Δ_1 real. There may be a phase-difference ϕ_0 over the junction which we defer to the right-hand superconductor. The angle θ corresponds to the angle of incidence of the quasiparticle approaching the superconductor. In the following we will use various forms of order parameters for $\Delta_1(\theta)$ and $\Delta_2(\theta)$ ranging from the s -wave case to the d -wave case. The d -wave superconductors are allowed to be rotated an angle α measured relative to the interface normal as described in Fig. 1.

In this paper we do not include the magnetic field. Including the magnetic field will screen any current on the length scale of the London penetration depth, forcing the current to flow next to surfaces/interfaces of superconductors. Neglecting screening effects is traditionally considered valid if the system under study has dimensions smaller than the London penetration depth. However, a finite system immediately raises questions about where the parallel current finally ends up. In this paper we do not address this question; instead we just note that a full treatment including screening effects will be required to understand how the parallel current is guided close to the interface of the d -wave superconductor.

Using the models discussed above for both the normal and the superconducting regions we solve the time-dependent Bogoliubov-de Gennes (BdG) equation for anisotropic superconductors

$$\int d^3x' \begin{pmatrix} h_0(\mathbf{x}, \mathbf{x}') & \Delta(\mathbf{x}, \mathbf{x}', t) \\ \Delta^*(\mathbf{x}, \mathbf{x}', t) & -h_0(\mathbf{x}, \mathbf{x}') \end{pmatrix} \begin{pmatrix} u(\mathbf{x}', t) \\ v(\mathbf{x}', t) \end{pmatrix} = i\hbar\partial_t \begin{pmatrix} u(\mathbf{x}, t) \\ v(\mathbf{x}, t) \end{pmatrix}, \quad h_0(\mathbf{x}, \mathbf{x}') = \delta(\mathbf{x} - \mathbf{x}') \left(\frac{p_{x'}^2}{2m} - \mu \right), \quad (3)$$

where μ is the chemical potential, and $\Delta(\mathbf{x}, \mathbf{x}', t)$ is the order parameter. Introducing a voltage the chemical potentials of the two reservoirs will be shifted relative to

each other, $eV = \mu_2 - \mu_1$. The natural energy reference level in a superconductor is the chemical potential. In order to establish a global energy reference level, a gauge transformation is performed as described in detail in Ref. 46. As a result of this transformation a phase difference appears over the junction obeying the Josephson relation $\partial_t\phi = 2eV/\hbar$. In other words, for our case with constant voltage we describe this time-dependent phase difference multiplying $\Delta_2(\theta)$ by $\exp(i2eVt/\hbar)$.

In Appendix A we solve Eq. (3) for the wave function $\Psi_\nu = (u_\nu, v_\nu)$ corresponding to an electron-like quasiparticle incident on the junction at an energy E_ν . Using this wave function we will in the next section calculate the current.

III. CALCULATING THE CURRENT

To calculate the current density \mathbf{j} we use the general formula

$$\mathbf{j} = \frac{e\hbar}{m} \sum_\nu [2f(E_\nu) - 1] \text{Im} \{u_\nu^* \nabla u_\nu + v_\nu^* \nabla v_\nu\}, \quad (4)$$

where we introduced the Fermi distribution function $f(E) = 1/[1 + \exp(E/k_B T)]$. The sum is over all scattering states originating from electron-like quasiparticles approaching the junction from the superconducting reservoirs at both negative and positive energies E_ν . There are different ways of writing the formula for the current density, but as shown in Appendix B they are all equivalent. Note that \mathbf{j} in our case may have a component in the y -direction (parallel to the junction). The wave function coefficients determined in Appendix A are introduced into the current formula of Eq. (4) in a way outlined below.

A. The x -current

We start by studying the current density j_x perpendicular to the junction. Since we consider a structure smaller than the London penetration depth (allowing us to neglect self-field effects) the current density will distribute uniformly over the junction. Therefore we may calculate the current density at any y -coordinate. Moreover, a conservation law for the current density assures that we may calculate j_x at any x -coordinate; it proves convenient to calculate the current density in the normal region (in our treatment to the left of the barrier in Fig. 1) between the superconducting reservoirs. The total perpendicular current I_x per ab -plane is then given by $I_x = L_y j_x$, where L_y is the length of the junction in the y -direction.

In Eq. (4) the quantum number ν is the wave vector \mathbf{k} of an electron-like quasiparticle approaching the junction. The direction could be thought of as another quantum number; we introduce $\tau = + (-)$ to indicate that the

quasiparticle is incident from the left (right). Therefore, using the wave function coefficients of Appendix A, the current per ab -plane is

$$I_x = L_y \frac{e\hbar}{m} \frac{k_F}{L_x L_y} \sum_{\mathbf{k}, \tau} \tau \cos(\theta_{\mathbf{k}}) T^\tau(\mathbf{k}) [2f(E_{\mathbf{k}}) - 1], \quad (5)$$

where the combination of k_F (the Fermi wavevector) and $\cos(\theta_{\mathbf{k}})$ ($\theta_{\mathbf{k}}$ is the angle of incidence for an electron-like quasiparticle incident with momentum \mathbf{k}) is produced by the x -derivative in Eq. (4). The factor $1/(L_x L_y)$ in the equation above normalizes the wavefunction of the incoming electronlike quasiparticle. In Eq. (5) we have introduced

$$T^\tau(\mathbf{k}) = \text{Re} \sum_{n,m} [(a_{L,2n+2m}^\tau)^* a_{L,2n}^\tau - (d_{L,2n+2m}^\tau)^* d_{L,2n}^\tau + (b_{L,2n+2m}^\tau)^* b_{L,2n}^\tau - (c_{L,2n+2m}^\tau)^* c_{L,2n}^\tau] \times e^{i\tau m 2eVt/\hbar} e^{i\tau m \phi_0}. \quad (6)$$

The set of states (electron-like quasiparticles) to sum over in Eq. (5) is illustrated in Fig. 11(c). In Eq. (6) n and m are integer numbers.

Next we change the sum over \mathbf{k} in Eq. (5) into an integration over d^2k . This produces a factor of $L_x L_y / (2\pi)^2$. Finally, changing the integration over d^2k into an integration over the superconducting energy $E = [(\hbar^2 k^2 / 2m - \mu)^2 + \Delta(\theta_{\mathbf{k}})^2]^{1/2}$ and the angle of incidence $\theta = \theta_{\mathbf{k}}$, we find the following expression for the current

$$\begin{aligned} \frac{I_x}{\sigma_0} &= \frac{eV}{\Delta_0} + \frac{1}{4D} \int_{-\pi/2}^{\pi/2} d\theta \cos \theta \int_{-\infty}^{\infty} \frac{dE}{\Delta_0} [2f(E) - 1] \\ &\quad \times \sum_{\tau} \tau N_\tau(E, \theta) T^\tau(E, \theta), \\ \sigma_0 &= L_y \frac{2^{5/2} e m^{1/2} E_F^{1/2} \Delta_0 D}{\hbar^2}, \end{aligned} \quad (7)$$

where $D = \int d\theta |t(\theta)|^2 \cos \theta / 2$ and E_F is the Fermi energy. The first term proportional to eV in Eq. (7) is due to referring energies of right-movers (left-movers) to the chemical potential of the left (right) superconductors. For details, see Refs. 44 and 46. We note that the second term of Eq. (7) is zero when all order parameters are put to zero. It is therefore reasonable to call this part the superconducting contribution to the current and the first part the normal contribution to the current.

It is now convenient to introduce $\Omega_m = m2eVt/\hbar + m\phi_0$. We then rewrite Eq. (7)

$$\frac{I_x}{\sigma_0} = \frac{eV}{\Delta_0} + \sum_m [A_{x,m} \cos \Omega_m + B_{x,m} \sin \Omega_m], \quad (8)$$

where $A_{x,m}$ and $B_{x,m}$ are given by

$$A_{x,m}(V) = \frac{1}{4D} \int_{-\pi/2}^{\pi/2} d\theta \cos \theta \int_{-\infty}^{\infty} \frac{dE}{\Delta_0} \tanh\left(\frac{-E}{2k_B T}\right)$$

$$\begin{aligned} &\times \sum_{\tau} \tau N_\tau(E) \text{Re} \{T_x^\tau(E, \theta, m)\}, \\ B_{x,m}(V) &= -\frac{1}{4D} \int_{-\pi/2}^{\pi/2} d\theta \cos \theta \int_{-\infty}^{\infty} \frac{dE}{\Delta_0} \tanh\left(\frac{-E}{2k_B T}\right) \\ &\quad \times \sum_{\tau} N_\tau(E) \text{Im} \{T_x^\tau(E, \theta, m)\}, \end{aligned} \quad (9)$$

together with

$$T_x^\tau(E, \theta, m) = \sum_{n=-\infty}^{\infty} [(a_{2n+2m}^\tau)^* a_{2n}^\tau - (d_{2n+2m}^\tau)^* d_{2n}^\tau + (b_{2n+2m}^\tau)^* b_{2n}^\tau - (c_{2n+2m}^\tau)^* c_{2n}^\tau]. \quad (10)$$

In Eq. (9) we write $2f(E) - 1 = \tanh(-E/2k_B T)$.

Finally, we introduce an amplitude $C_{x,m} = (A_{x,m}^2 + B_{x,m}^2)^{1/2}$ and a phase $\alpha_{x,m} = \arctan(B_{x,m}/A_{x,m})$ in order to write the current as

$$\begin{aligned} \frac{I_x}{\sigma_0} &= \frac{eV}{\Delta_0} + \sum_m C_{x,m} \cos(\Omega_m - \alpha_{x,m}) \\ &= \frac{eV}{\Delta_0} + \sum_m C_{x,m} e^{i(\Omega_m - \alpha_{x,m})}, \end{aligned} \quad (11)$$

where we in the last step used the symmetries $A_{x,-m} = A_{x,m}$, $B_{x,-m} = -B_{x,m}$ giving $C_{x,-m} = C_{x,m}$, $\alpha_{x,-m} = -\alpha_{x,m}$. These symmetries are due to the relation $T^\tau(E, \theta, -m) = [T^\tau(E, \theta, m)]^*$. Note that the last expression in Eq. (11) is equal to Eq. (1).

Studying the phases $\Omega_m - \alpha_{x,m}$ in Eq. (11) we see that for $m = 0$ they are all zero implying that the zero-frequency component does not depend on the phase difference ϕ_0 over the junction. For the components with $m \neq 0$, we see that we can arrange the phases as $\Omega_m - \alpha_{x,m} = m\omega_J(t - t_0)$, where $t_0 = (\alpha_{x,m}/m - \phi_0)/\omega_J$ can be thought of as the time when the measurement starts. It will therefore be of no importance for the different current components in the following discussion, which rather focuses on the amplitude C_m .

B. The y -current

We now move on to study the y -current (current parallel to the junction). Below we will see that in general the y -current density $j_y(x)$ (current per ab -plane and unit length in the x -direction) depends on the x -direction. To stress this dependence on x we have chosen to discuss the parallel current in terms of the current density j_y .

The analysis of the parallel current density follows closely the one presented for the perpendicular current above. There are four main differences: first, the derivative with respect to y in Eq. (4) now leads to a factor of $\sin \theta$ (instead of $\cos \theta$); second, there will only be plus signs in the equation corresponding to Eq. (10); third, there is an oscillating term in j_y ; fourth, there is no normal contribution to the parallel current as in the perpendicular case discussed above.

Therefore, we write down (suppressing the x -dependence) the parallel current density j_y as

$$j_y(V, t) = \sum_m j_{y,m}(V) e^{im\omega t} \quad (12)$$

with the components defined as

$$\begin{aligned} \frac{j_{y,0}(V)}{(\sigma_0/L_y)} &= A_{y,0}(V), \\ \frac{j_{y,m}(V)}{(\sigma_0/L_y)} &= C_{y,m}(V) e^{i(m\phi_0 - \alpha_{y,m})}, \quad m \neq 0 \\ C_{y,m}(V) &= \sqrt{A_{y,m}^2(V) + B_{y,m}^2(V)}, \\ \alpha_{y,m} &= \arctan \frac{B_{y,m}(V)}{A_{y,m}(V)}, \end{aligned} \quad (13)$$

together with

$$\begin{aligned} A_{y,m}(V) &= \frac{1}{4D} \int_{-\pi/2}^{\pi/2} d\theta \sin \theta \int_{-\infty}^{\infty} \frac{dE}{\Delta_0} \tanh \left(\frac{-E}{2k_B T} \right) \\ &\quad \times \sum_{\tau} \tau N_{\tau}(E) \text{Re} \{ T_y^{\tau}(E, \theta, m) \}, \\ B_{y,m}(V) &= -\frac{1}{4D} \int_{-\pi/2}^{\pi/2} d\theta \sin \theta \int_{-\infty}^{\infty} \frac{dE}{\Delta_0} \tanh \left(\frac{-E}{2k_B T} \right) \\ &\quad \times \sum_{\tau} N_{\tau}(E) \text{Im} \{ T_y^{\tau}(E, \theta, m) \}, \\ T_y^{\tau}(E, \theta, m) &= \sum_{n=-\infty}^{\infty} \{ (a_{2n+2m}^{\tau})^* a_{2n}^{\tau} + (b_{2n+2m}^{\tau})^* b_{2n}^{\tau} \\ &\quad + (c_{2n+2m}^{\tau})^* c_{2n}^{\tau} + (d_{2n+2m}^{\tau})^* d_{2n}^{\tau} \\ &\quad + 2 [(a_{L,n+m}^{\tau})^* d_{L,n}^{\tau} + (b_{L,n+m}^{\tau})^* c_{L,n}^{\tau}] \\ &\quad \times e^{-2ik_F \cos \theta x} \}. \end{aligned} \quad (14)$$

The last term in $T_y^{\tau}(E, \theta, m)$ oscillates on a scale $1/k_F$ and would be hard to observe in an experiment. We therefore drop it when we calculate the parallel current. This is reasonable since j_y is a current density: To get the total current we should integrate in the x -direction. The oscillating term will then average to zero. Dropping the oscillating term, j_y will no longer be continuous when passing the barrier: the value of j_y will be different at $x = 0^+$ and $x = 0^-$ (with the δ -function barrier located at $x = 0$). However, we have checked that the $m = 0$ component of j_y is continuous if the oscillating term is included. For completeness we will in this paper give (the average value of) the current density on both sides of the barrier, denoted j_{yL} and j_{yR} , respectively. For the ballistic case ($Z = 0$) we have $j_{yL} = j_{yR}$.

In the next section we discuss $C_{x,m}(V)$ and $C_{y,m}(V)$ for some configurations of superconductors.

IV. RESULTS AND DISCUSSION

We will in this section present curves only for positive voltage: in Appendix C we show that the current is odd in voltage.

We start by discussing the results for the $m = 0$ term of the sum in Eq. (1). In Fig. 5 we have plotted the $I - V$ curves for different values of the temperature. For zero temperature there is a peak in the current for some orientations due to resonant transport through MGS.¹³⁻¹⁵ This feature (resulting in negative differential conductance) is especially pronounced for arrangements where one superconductor is an s -wave superconductor and the other one is a d -wave superconductor with orientation angle $\alpha = \pi/4$. In Fig. 5(a)-(b) we study how temperature influences the current peak appearing at a voltage $eV = \Delta_s$. We find that the peak is rather robust up to relatively high temperatures, such as $0.5T_{cs}$ shown in the figure, where T_{cs} is the critical temperature of the s -wave superconductor. In Fig. 5 we have taken into account the fact that the s -wave superconducting gap is reduced when the temperature is increased according to the theory by Bardeen, Cooper, and Schrieffer.⁴⁷ This is the reason for the shift of the peak towards lower voltage when the temperature is increased. The d -wave order parameter, on the other hand, is assumed not to be affected by the temperature variations, since T_c for HTS compounds in general is considerably higher compared to conventional superconductors.

It is interesting to compare with the NS junction,¹² where it has been found that the presence of MGS induces a dramatic increase of current for low voltage resulting in ZBCP. This structure is more sensitive to temperature than the current peak of the $s|d_{\pi/4}$ -junction discussed in the paragraph above. The reason for this greater sensitivity is the density of states: it is well known that MGS are located at the Fermi energy on the d -wave side. This means that quasiparticles incident from the normal side will reach MGS for any small voltage. This, however, is in great contrast to the $s|d_{\pi/4}$ -case, where MGS on the d -wave side may only be reached from the s -wave side at a voltage greater than Δ_s simply because the superconducting density of states is zero for subgap energies. The conclusion is therefore that the NS case will be more affected by thermal smearing introduced by the Fermi functions, since this smearing is centralized around the Fermi energy. This argument breaks down at temperatures larger than the s -wave gap, taking place close to T_c of the s -wave superconductor.

An interesting paper⁷ has recently appeared studying experimentally the system corresponding to the case depicted in Fig. 5. In that paper two sets of curves are presented: first, Fig. 4(a) of Ref. 7 denoted here by (i); second, Fig. 4(b) of Ref. 7 denoted here by (ii). While the results of (i) are in agreement with the picture outlined in our Fig. 5, the curves of (ii) are not easily understood from our calculations. The critical point for not having

agreement is the fact that in (ii) there is no opening of the superconducting s -wave gap corresponding to the Pb electrode to be found.

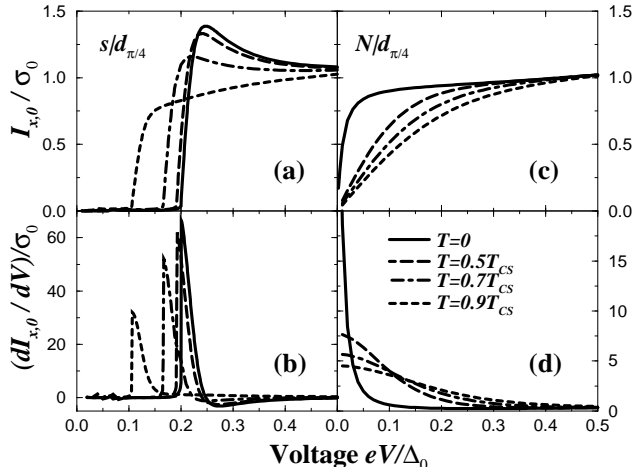


FIG. 5. Current-voltage curves and differential conductance-voltage curves for $s|d_{\pi/4}$ [(a) and (b) respectively] and $N|d_{\pi/4}$ junctions [(c) and (d) respectively] are shown for some temperatures. The zero bias conductance peak present for the $N|d$ case is moved to finite bias $eV = \Delta_s(T)$ when the counter electrode is an s -wave superconductor. In addition negative conductance appears. The peak moves to smaller voltage when T is close to T_{cs} since Δ_s is reduced by temperature according to the BCS theory. The figure demonstrates that the peak is less sensitive to temperature for the $s|d$ junction compared to the $N|d$ junction. The barrier strength is $Z=5$, and $\Delta_s(T=0) = 0.2\Delta_0$.

Very recently an investigation of ZBCP in bicrystal grain boundary junctions have appeared,^{9,10} discussing (among other things) a geometry corresponding to $\alpha_1 = -\alpha_2 = 18.4^\circ$, in which ZBCP was found. In our calculations ZBCP can only be found in rather transparent (small Z) $d|d$ junctions, as shown in Fig 6. The reason for this is that the scattering states start from the bulk where there are no superconducting density of states close to zero energy except for angles corresponding to the gap nodes of the d -wave superconductor. For small voltage, the MGS can only be reached by the scattering states from those angles, making the MGS contribution very limited in the angle average. Broadening of MGS due to reduced barrier height Z (which is incorporated in our treatment from the start) increases the range of angles from which the scattering states may reach MGS. For low barrier height the width of the MGS becomes comparable to the gap making the junction ballistic^{37,46} for scattering states starting near the gap edges, allowing MAR to contribute massively to the current. The current then takes a finite value for small voltage and a huge ZBCP appears. It is important to have MGS on both sides of the barrier for this effect; otherwise, the number of AR will be reduced, resulting in a smaller current contribution. Fig. 6 demonstrates that at a barrier strength $Z = 1$, corresponding to an averaged transparency $D = 0.38$, the

ZBCP has disappeared within our model: for this barrier strength the width of the MGS is not high enough to give large current at small voltage.

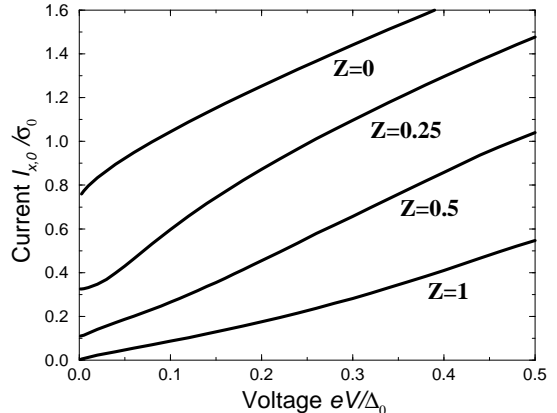


FIG. 6. Current-voltage curves are plotted for the $d_{\pi/8}|d_{-\pi/8}$ junction with barrier strengths $Z = 0, 0.25, 0.5,$ and 1 . The finite value of the current at small voltage for low (but finite) barrier strength is due to resonant transport through MGS making the junction ballistic. For comparison, the ballistic ($Z = 0$) curve is shown (no MGS in the ballistic case) where there is always a finite current in the zero-bias limit.

A related issue is the case $\alpha_1 = \alpha_2 = 45^\circ$ discussed in Ref. 13. Also in this case a combination of broadened MGS on both sides of the barrier and MAR give rise to ZBCP for small (e. g. $Z = 0.25$) barrier strengths, although the peak is not as sharp as for $d_{\pi/8}|d_{-\pi/8}$. As explained above there are no scattering states at zero energy except for the angles corresponding to the gap nodes. Since for the orientation $\alpha_1 = \alpha_2 = 45^\circ$ the gap nodes are geometrically lined up against each other, the influence of MGS will be less dramatic compared to the case discussed in the previous paragraph. An interesting paper, mainly on calculations in the tunneling limit, introduces phenomenologically an imaginary part of the energy, corresponding to broadening of the MGS.⁴⁸ (In our calculation there is no imaginary part of the energy.) Due to the imaginary part ZBCP was found in the case $\alpha_1 = \alpha_2 = 45^\circ$.⁴⁸ The difference compared to our work is that in our work the broadening is not introduced phenomenologically; contrary, it is microscopically described in terms of reduced strength of the barrier.

We now continue to discuss the $m \neq 0$ ac current components of Eq. (1). In Fig. 7 we show some results for current density for both the perpendicular (x) and parallel (y) direction. The curves shown in Fig. 7 are for the ballistic ($Z = 0$) case. The ballistic case is rather restricted; however, it will prove very useful for us to illustrate some important properties of $d_{\alpha_1=0}|d_{\alpha_2}$ junctions in the ac case. These qualitative properties carry over to the non-ballistic case in a straightforward manner. Quantitatively, the curves will look different in the

presence of normal scattering.

We start by discussing $\alpha_2 = \pi/4$. In Fig. 7 we plot the magnitude C_m of the ac components. It is then possible for us to show how the disappearance of the ac components in the x -direction¹⁷ will be complemented by the appearance of the corresponding ac components in the y -direction as seen in Fig. 7(b) and (e). The detailed explanation for this effect is given in Appendix C and is good for any value of Z . The main point is that the current is calculated from an integration over angles θ , where the integrand is composed of two functions. The first function is $\cos(\theta)$ [$\sin(\theta)$] produced by a derivative in x (y) in Eq. (4). The other function can be proved to be odd (even) in θ for odd (even) m . It is now clear that the combination of these two functions integrated will result in zero current density in the x (y) direction for odd (even) m . This scenario is confirmed in detail from the calculation presented in Fig. 7. We note in passing that the $m = 0$ component has a finite current in the limit $eV \rightarrow 0$ as discussed in Appendix D.

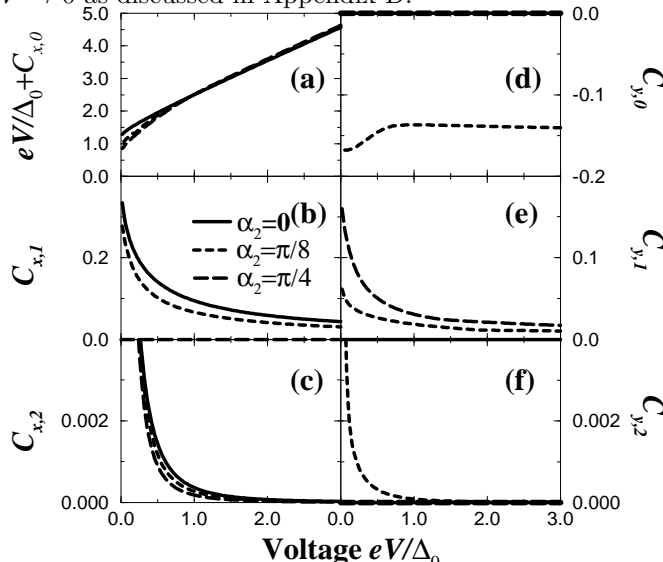


FIG. 7. The first three components ($m = 0, 1, 2$) of the perpendicular current [(a)-(c)] and the parallel current [(d)-(f)] is shown for the $d_0|d_{\alpha_2}$ junction for three different orientations of the right superconductor. The odd components of the perpendicular current is suppressed when the orientation angle α_2 is changed from 0 towards $\pi/4$ (and zero at $\pi/4$). At the same time the odd component of the parallel current is enhanced. We also see that all components of the parallel current vanishes for the orientation $\alpha_2 = 0$. The barrier strength is $Z = 0$ and the temperature is zero.

Next we discuss the parallel current density in the presence of normal scattering. We specialize to the $d_0|d_{\pi/8}$ junction with $Z = 1$ for zero temperature. The curves depicted in Fig. 8 are the $m = 0$ component calculated in the normal regions. As explained in Section III the average current density in the left side differs from the right side of the barrier. We note that the large-voltage limit of the curves in Fig. 8 is of the order of the perpendicular excess current density, implying a saturation at large

voltages. Below we indicate which side the current densities are to be associated with by adding an index L/R for left/right whenever the side of the junction matters.

The fine structure in Fig. 8 is due to subharmonic gap structure of the same origin as in the case of perpendicular current.^{13,17}

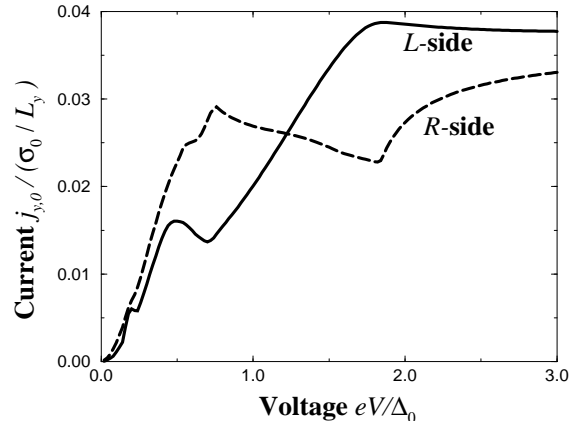


FIG. 8. Parallel current for the $d_0|d_{\pi/8}$ junction to the left and to the right of the barrier. The barrier strength is $Z=1$ and the temperature is zero.

The large-voltage limit of the parallel current density can be calculated analytically in the ballistic limit, see Appendix D. For the orientation $\alpha_1 = 0$ and $\alpha_2 = \pi/8$, the value of the large-voltage limit of the parallel current density will be negative. In Fig. 9 we plot the dependence of the large-voltage limit of the parallel current density on the barrier strength Z . The result is that we get a sign change at a rather small value of Z . The sign (change) can be qualitatively understood by studying Fig. 3 in combination with Eq. (D1). We see that Fig. 3 approximately represent the case $\alpha_2 = \pi/8$. For $Z = 0$ the current contributions for each angle of incidence will be averaged by the function $\sin\theta$. We see in Fig. 3 that the largest gap appears at negative angles where $\sin\theta$ is negative. The value of the integral in Eq. (D1) will therefore be negative, since only the absolute value of the gap appears in Eq. (D1). Introducing normal scattering means that small angles of incidence are more strongly weighted (note the structure of transmission amplitude $t(\theta)$). In Fig. 3 we see that the largest gap will be at positive angles in this case, implying a positive current since $\sin\theta$ is positive for positive angles. In addition, the normal scattering will introduce contributions from the gap $\tilde{\Delta}_2 = \Delta_2(-\alpha_2)$ at the expense of Δ_2 . One can show that for the $d_0|d_{\alpha_2}$ junction the relation $j_y(-\alpha_2) = -j_y(\alpha_2)$ holds for all Z , implying that the introduction of $\tilde{\Delta}_2$ gives contributions with the positive sign. The inset in Fig. 9 illustrates the relation $j_y(-\alpha_2) = -j_y(\alpha_2)$. In conclusion, the positive contributions will quickly dominate over negative contributions in the angle average when we change Z from zero to finite values.

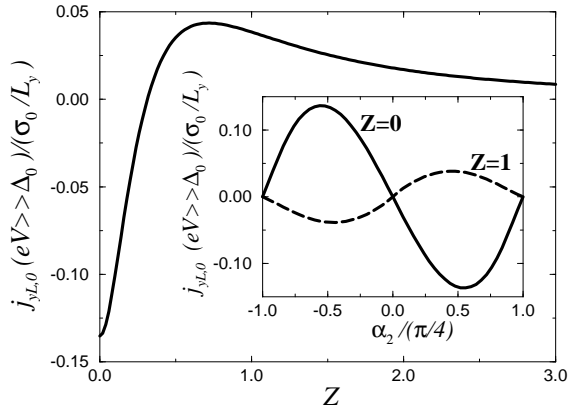


FIG. 9. We show the current density parallel to the junction interface in the limit $eV \gg \Delta_0$ as a function of the barrier strength for the orientation $\alpha_1 = 0$ and $\alpha_2 = \pi/8$. In the inset we show the dependence on the misorientation angle α_2 of the right superconductor for the barrier strengths $Z = 0$ and $Z = 1$ keeping $\alpha_1 = 0$. Note that the factor D (which is Z -dependent) is included in σ_0 , giving a larger normalized value of the current for non-zero Z . Zero temperature is assumed in all cases.

Finally, we show in Fig. 10 some $I - V$ curves for the $N|d_\alpha$ junction for several barrier strengths and orientations α . The curves demonstrate what is illustrated in Fig. 3: for almost any orientation (the exceptions are $\alpha_2 = n\pi/4$) there is a net parallel current density. In our model the parallel current density will be present everywhere in the normal region. This might not be surprising since we do not take into account any impurity scattering in the bulk.

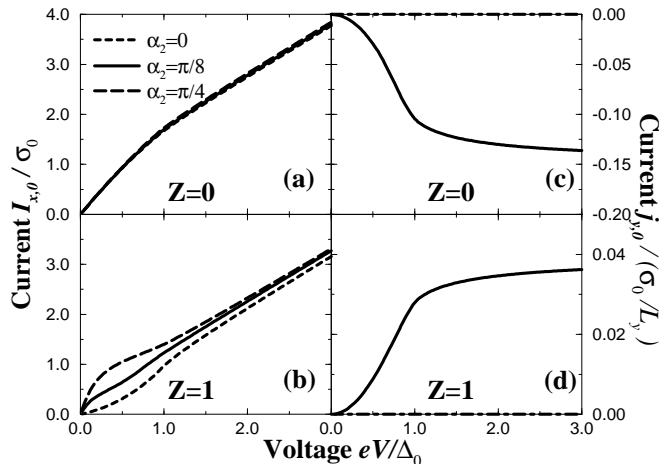


FIG. 10. Currents for the $N|d_\alpha$ junction at barrier strengths $Z = 0$ and $Z = 1$. In (a)-(b) we show the perpendicular current I_x flowing through the junction and in (c)-(d) we show the parallel current density j_y . In (b) we see that the zero bias conductance peak grows up when we rotate the orientation of the superconductor from $\alpha_2 = 0$ to $\alpha_2 = \pi/4$. The parallel current only exists when $\alpha_2 \neq n\pi/4$, as seen in (c)-(d).

An important limitation of the present work is that we do not include magnetic field. From a calculation with a self-consistent magnetic field one should expect that the parallel current density is screened out in the superconductors on the length scale of the London penetration depth. This means that our results for the parallel current density presented in Figs. 7 to 10 are only valid for systems with dimensions smaller than the London penetration depth.

V. SUMMARY

In this paper we have studied the ac Josephson effect for planar superconducting d -wave junctions. The presence of zero-energy midgap states (MGS) at interfaces of d -wave superconductors for some orientations influence the current-voltage curves (the zeroth order ac component), since MGS open up additional channels for current flow. We have primarily discussed two aspects of MGS in this paper. First, our results feature current peaks at finite voltage (resulting in negative differential conductance) in the $S_1|S_2$ case.¹³ We have in this paper explored how sensitive this current peak is to temperature. We have also discussed how well our calculations compare with an experiment:⁷ some curves of this experiment compare well with our results; however, there is in Ref. 7 a set of curves which we find difficult to understand within the framework of the model we are using. The second aspect relates to a recent experiment on $d_\alpha|d-\alpha$ junctions,^{9,10} where zero-bias conductance peaks (corresponding to large current increase for small voltage) have been found. Our model explains these experimental results in terms of resonant transport through MGS if the grain boundary is rather transparent, allowing multiple Andreev reflections to contribute hugely to the current for low voltage.

An interesting feature of superconducting d -wave junctions is the possibility to have parallel current density at the interface of the two electrodes. We explain the reason for this effect for the ac Josephson effect. We also demonstrate how the disappearance of the odd ac components for the perpendicular current¹⁷ in some orientations is complemented by appearance of odd ac components in the direction parallel to the junction.

Moreover, we have given a fairly complete account of our method which is applicable to all types of junctions: all the way from the ballistic (no barrier) to the insulating case. We have also discussed how different current formulas previously used relate to each other.

ACKNOWLEDGMENTS

It is a pleasure to thank V. S. Shumeiko and M. Moraghebi for many useful discussions on this work. M. H. also acknowledges discussions with P. Johansson. Finally,

we thank L. Alff for explaining some geometrical aspects of the grain boundary experiments performed in Ref. 9.

APPENDIX A: SOLUTION OF THE BOGOLIUBOV-DE GENNES EQUATION

The complicated integral operator makes exact solutions of Eq. (3) not easily accessible. Therefore, we solve Eq. (3) approximately by an ansatz in each region of the following type:

$$\begin{pmatrix} u(\mathbf{x}, t) \\ v(\mathbf{x}, t) \end{pmatrix} = \sum_{\mathbf{k}} A_{\mathbf{k}} e^{i\mathbf{k}\cdot\mathbf{x}} \begin{pmatrix} u_{\mathbf{k}} \\ v_{\mathbf{k}} \end{pmatrix} e^{-iE_{\mathbf{k}}t/\hbar}, \quad (\text{A1})$$

where the Fourier sum over different frequencies reflects the fact that there is a time dependence in the order parameter after a global reference level is chosen as described in Section II. We follow the standard treatment when approximating the integral operator of Eq. (3): the center of mass coordinate $\mathbf{R} = (\mathbf{x} + \mathbf{x}')/2$ and the relative mass coordinate $\mathbf{r} = \mathbf{x} - \mathbf{x}'$ are introduced. This means that in these new coordinates the order parameter is written $\Delta(\mathbf{x}, \mathbf{x}') = \tilde{\Delta}(\mathbf{r}, \mathbf{R})$. The integral operator of Eq. (3) is now approximated as

$$\begin{aligned} \int d\mathbf{x}' \Delta(\mathbf{x}, \mathbf{x}') v(\mathbf{x}', t) &= \int d\mathbf{r} \tilde{\Delta}(\mathbf{r}, \mathbf{x} - \mathbf{r}/2) v(\mathbf{x} - \mathbf{r}, t) \\ &\approx \sum_{\mathbf{k}} \Delta(\mathbf{k}, \mathbf{x}) A_{\mathbf{k}} v_{\mathbf{k}} e^{i\mathbf{k}\cdot\mathbf{x}} e^{-iE_{\mathbf{k}}t/\hbar}, \end{aligned} \quad (\text{A2})$$

where we have introduced the Fourier transform $\Delta(\mathbf{k}, \mathbf{R})$ of the order parameter $\tilde{\Delta}(\mathbf{r}, \mathbf{R})$. In Eq. (A2) we approximated $\tilde{\Delta}(\mathbf{r}, \mathbf{x} - \mathbf{r}/2) \approx \tilde{\Delta}(\mathbf{r}, \mathbf{x})$, valid since $\tilde{\Delta}(\mathbf{r}, \mathbf{x})$ is assumed to be a slow (fast) function in \mathbf{x} (\mathbf{r}). Since in the weak-coupling limit the pair potential is expected to be non-zero only close to k_F , one can replace the momentum by an angle θ . The approximation made in Eq. (A2) neglects terms of the order $(k_F \xi_0)^{-1}$ and is called the quasi-classical approximation.⁴⁵

Before solving the time-dependent BdG equation it is convenient to introduce some notational simplifications. First we define the BCS coherence factors

$$\begin{aligned} \frac{v_i(E, \theta)}{u_i(E, \theta)} &= \frac{E - \text{sgn}(E) \sqrt{E^2 - \Delta_i(\theta)^2}}{\Delta_i(\theta)}, \quad |E| > |\Delta_i(\theta)| \\ \frac{v_i(E, \theta)}{u_i(E, \theta)} &= \frac{E - i \sqrt{\Delta_i(\theta)^2 - E^2}}{\Delta_i(\theta)}, \quad |E| < |\Delta_i(\theta)| \end{aligned} \quad (\text{A3})$$

where $|u_i|^2 + |v_i|^2 = 1$ and $i = 1, 2$ refers to superconductor 1 and 2. Using this definition, one can express the Andreev reflection amplitude at superconductor i as $A_i(E_n, \theta) \equiv A_{i,n} = v_i(E_n, \theta)/u_i(E_n, \theta)$, where $E_n = E + neV$. The transmission amplitude for an electron-like quasiparticle at energy E and angle θ from superconductor i to enter the electron branch in the normal region is

$J_i(E, \theta) \equiv J_i = (u_i^2(E, \theta) - v_i^2(E, \theta))/u_i(E, \theta)$. An important notational detail in this paper are the barred quantities: these are to be associated with the angle $\bar{\theta} = \pi - \theta$.

To solve the time-dependent BdG equation we follow the method worked out for the s -wave case^{38,39,46,44} and further generalized to the anisotropic case.^{13,17} We use the boundary condition that far away from the junction the wave function corresponds to an electron-like quasiparticle incident on the junction from one side at an energy E and an angle θ . Thanks to symmetries of the BdG equation it is enough to study these electron-like quasiparticle solutions as explained in Appendix B. The incident quasiparticle gives in general rise to both reflected and transmitted waves. Therefore, we start writing down the wave function in the left superconductor as (corresponding to a quasiparticle incident on the junction from the left)

$$\begin{aligned} \Psi_{S_1}^{\rightarrow} &= \sum_n \left[\delta_{n,0} \begin{pmatrix} u_1(E_n, \theta) \\ v_1(E_n, \theta) \end{pmatrix} e^{i\mathbf{q}^e \cdot \mathbf{x}} \right. \\ &+ b_{1,n} \begin{pmatrix} v_1(E_n, \theta) \\ u_1(E_n, \theta) \end{pmatrix} e^{i\mathbf{q}^h \cdot \mathbf{x}} \\ &\left. + d_{1,n} \begin{pmatrix} \bar{u}_1(E_n, \theta) \\ \bar{v}_1(E_n, \theta) \end{pmatrix} e^{i\bar{\mathbf{q}}^e \cdot \mathbf{x}} \right] e^{-i(\frac{E_n t}{\hbar} + \frac{n\phi_0}{2})}. \end{aligned} \quad (\text{A4})$$

where $\mathbf{q}^{e/h}$ corresponds to the wave vector of electron/hole-like quasiparticles. For the wave vectors above (and in the following) we use the notation $\mathbf{q} = (q_x, q_y) = q(\cos \theta, \sin \theta)$ and $\bar{\mathbf{q}} = (-q_x, q_y) = q(\cos \bar{\theta}, \sin \bar{\theta})$, where $\bar{\theta} = \pi - \theta$ corresponds to the angle after normal scattering. We will approximate the magnitude of any wave vector in this paper as the Fermi wave vector, $q \approx k_F$. Again, all barred quantities are to be associated with the angle $\bar{\theta}$. In the voltage case the injected quasiparticle goes through multiple Andreev reflections (MAR). The wavefunction therefore contains sidebands at energies $E_n = E + neV$, where n is an even integer.

In the normal region the wave function to the left and right of the barrier is

$$\Psi_L^{\rightarrow} = \sum_n \begin{pmatrix} a_{L,n} e^{i\mathbf{k}^e \cdot \mathbf{x}} + d_{L,n} e^{i\bar{\mathbf{k}}^e \cdot \mathbf{x}} \\ b_{L,n} e^{i\mathbf{k}^h \cdot \mathbf{x}} + c_{L,n} e^{i\bar{\mathbf{k}}^h \cdot \mathbf{x}} \end{pmatrix} e^{-i(\frac{E_n t}{\hbar} + \frac{n\phi_0}{2})}, \quad (\text{A5})$$

$$\Psi_R^{\rightarrow} = \sum_n \begin{pmatrix} a_{R,n} e^{i\mathbf{k}^e \cdot \mathbf{x}} + d_{R,n} e^{i\bar{\mathbf{k}}^e \cdot \mathbf{x}} \\ b_{R,n} e^{i\mathbf{k}^h \cdot \mathbf{x}} + c_{R,n} e^{i\bar{\mathbf{k}}^h \cdot \mathbf{x}} \end{pmatrix} e^{-i(\frac{E_n t}{\hbar} + \frac{n\phi_0}{2})}, \quad (\text{A6})$$

respectively. The wave function of the right superconductor is

$$\begin{aligned} \Psi_{S_2}^{\rightarrow} &= \sum_n \left\{ \left[a_{2,n} \begin{pmatrix} u_2(E_n, \theta) e^{i\frac{\phi_0}{2}} e^{i(\frac{eVt}{\hbar})} \\ v_2(E_n, \theta) e^{-i\frac{\phi_0}{2}} e^{-i(\frac{eVt}{\hbar})} \end{pmatrix} e^{i\mathbf{p}^e \cdot \mathbf{x}} \right. \right. \\ &+ c_{2,n} \begin{pmatrix} \bar{v}_2(E_n, \theta) e^{i\frac{\phi_0}{2}} e^{i(\frac{eVt}{\hbar})} \\ \bar{u}_2(E_n, \theta) e^{-i\frac{\phi_0}{2}} e^{-i(\frac{eVt}{\hbar})} \end{pmatrix} e^{i\bar{\mathbf{p}}^h \cdot \mathbf{x}} \left. \right] \\ &\times e^{-i(\frac{E_n t}{\hbar} + \frac{n\phi_0}{2})} \left. \right\}. \end{aligned} \quad (\text{A7})$$

In the wave functions written down in Eqs. (A4)-(A7) we have explicitly factored out the dependence on the phase ϕ_0 for convenience, making the coefficients a , b , c , and d all independent of ϕ_0 . In the final expression for the current, however, the phase ϕ_0 will reappear.

In the following we solve the matching problem. We have three interfaces where the wave functions and derivatives in Eqs. (A4)-(A7) are to be matched. The procedure is the same as the one carried out in Refs. 44 and 46. When matching at the left interface between superconductor 1 and the left normal region we get

$$a_{L,n} = A_{1,n}b_{L,n} + J_1\delta_{n,0}, \quad c_{L,n} = \bar{A}_{1,n}d_{L,n}, \quad (\text{A8})$$

after eliminating coefficients pertaining to the left superconductor.

Repeating the procedure at the interface between the right normal region and superconductor 2 we have

$$b_{R,n+2} = A_{2,n+1}a_{R,n}, \quad d_{R,n} = \bar{A}_{2,n+1}c_{R,n+2}. \quad (\text{A9})$$

We have now eliminated coefficients related to the superconducting regions.

It now remains to match the wave functions in the normal region at the scattering center. This procedure may be expressed in terms of the scattering matrix

$$S_e(\theta) = \begin{pmatrix} r(\theta) & t(\theta) \\ t(\theta) & -r^*(\theta)t(\theta)/t^*(\theta) \end{pmatrix}. \quad (\text{A10})$$

The scattering matrix for holes is $S_h(\theta) = S_e^*(\theta)$. The scattering matrix relates incoming waves with outgoing waves. As outlined in Ref. 44 for the case of s -wave superconductors with different gaps, the wave-function coefficients of the left and right side of the normal region fulfill [suppressing the θ -dependence of $r(\theta)$ and $t(\theta)$]

$$d_{L,n} = rA_{1,n}b_{L,n} + rJ_1\delta_{n,0} + t\bar{A}_{2,n+1}c_{R,n+2}, \quad (\text{A11})$$

$$a_{R,n} = tA_{1,n}b_{L,n} + tJ_1\delta_{n,0} - \frac{r^*t}{t^*}\bar{A}_{2,n+1}c_{R,n+2}, \quad (\text{A12})$$

$$b_{L,n} = r^*\bar{A}_{1,n}d_{L,n} + t^*A_{2,n-1}a_{R,n-2}, \quad (\text{A13})$$

$$c_{R,n} = t^*\bar{A}_{1,n}d_{L,n} - \frac{rt^*}{t}A_{2,n-1}a_{R,n-2}. \quad (\text{A14})$$

Using Eqs. (A8)-(A14) we solve for d_L . As a result we find the following recursive relation:

$$\alpha_n d_{L,n+2} + \beta_n d_{L,n} + \gamma_n d_{L,n-2} = rJ_1\delta_{n,0}, \quad (\text{A15})$$

where

$$\begin{aligned} \alpha_n &= -|t|^2 \frac{\bar{A}_{2,n+1}\bar{A}_{1,n+2}}{1 - A_{2,n+1}\bar{A}_{2,n+1}} \\ \beta_n &= 1 - A_{1,n}\bar{A}_{1,n} + |t|^2 \left(\frac{A_{1,n}\bar{A}_{1,n}}{1 - A_{2,n-1}\bar{A}_{2,n-1}} \right. \\ &\quad \left. + \frac{A_{2,n+1}\bar{A}_{2,n+1}}{1 - A_{2,n+1}\bar{A}_{2,n+1}} \right), \quad \gamma_n = -|t|^2 \frac{A_{2,n-1}A_{1,n}}{1 - A_{2,n-1}\bar{A}_{2,n-1}}. \end{aligned} \quad (\text{A16})$$

The coefficient b_L is determined from

$$\begin{aligned} b_{L,n+2} &= \frac{1}{r(1 - A_{2,n+1}\bar{A}_{2,n+1})} (|t|^2 A_{2,n+1}d_{L,n} \\ &\quad + \bar{A}_{1,n+2}(|r|^2 - A_{2,n+1}\bar{A}_{2,n+1})d_{L,n+2}). \end{aligned} \quad (\text{A17})$$

Eqs. (A15)-(A17) and Eq. (A8) above, together with the boundary condition that the coefficients should go to zero as n goes to plus or minus infinity, determine the wave function completely in the region to the left of the barrier.¹³

Studying Eqs. (A16)-(A17) we notice some unnecessary singularities, which we may get rid of by defining

$$\begin{aligned} d'_{L,n} &= d_{L,n}/(r\eta_{n-1}\eta_{n+1}), \\ \eta_n &= 1 - A_{2,n}\bar{A}_{2,n}, \end{aligned} \quad (\text{A18})$$

and

$$\begin{aligned} \alpha'_n &= \eta_{n+1}\eta_{n+3}\alpha_n, \\ \beta'_n &= \eta_{n-1}\eta_{n-3}\beta_n, \\ \gamma'_n &= \eta_{n-3}\eta_{n-1}\gamma_n. \end{aligned} \quad (\text{A19})$$

The coefficient b_L is determined from

$$\begin{aligned} b_{L,n+2} &= |t|^2 A_{2,n+1}\eta_{n-1}d'_{L,n} \\ &\quad + \bar{A}_{1,n+2}(|r|^2 - A_{2,n+1}\bar{A}_{2,n+1})\eta_{n+3}d'_{L,n+2}. \end{aligned} \quad (\text{A20})$$

Using the primed quantities above there is a new recursive relation

$$\alpha'_n d'_{L,n+2} + \beta'_n d'_{L,n} + \gamma'_n d'_{L,n-2} = J_1\delta_{n,0}, \quad (\text{A21})$$

which is more suitable to handle from a numerical point of view. Solving for d'_L we use Eq. (A18) to get the original wave function coefficient d_L .

To solve Eq. (A21) we use a method previously introduced in the s -wave case.³⁸ First, we introduce

$$x_n = \begin{cases} d'_{L,n}/d'_{L,n-2}, & n > 0 \\ d'_{L,n}/d'_{L,n+2}, & n < 0, \end{cases} \quad (\text{A22})$$

leading to

$$\begin{aligned} \alpha'_n x_{n+2} + \beta'_n + \gamma'_n \frac{1}{x_n} &= 0, \quad n > 0 \\ \alpha'_n \frac{1}{x_n} + \beta'_n + \gamma'_n x_{n-2} &= 0, \quad n < 0, \end{aligned} \quad (\text{A23})$$

together with

$$d'_{L,0}(\alpha'_0 x_2 + \beta'_0 + \gamma'_0 x_{-2}) = J_1. \quad (\text{A24})$$

Rearranging Eq. (A23) we get a continued fraction expansion

$$\begin{aligned} x_n &= \frac{-\gamma'_n}{\beta'_n + \alpha'_n x_{n+2}}, \quad n > 0, \\ x_n &= \frac{-\alpha'_n}{\beta'_n + \gamma'_n x_{n-2}}, \quad n < 0. \end{aligned} \quad (\text{A25})$$

The continued fraction expansion can be evaluated by a routine in Ref. 49 giving us a good approximation for $x_{n_{large}}$, or be truncated at a large $n = n_{large}$. It turns out that the truncation method is often very accurate, especially if the barrier strength Z is large. Having calculated x_n we get all d'_n from the relations

$$d'_{L,n} = \begin{cases} x_n x_{n-2} \dots x_2 d'_{L,0}, & n > 0 \\ x_n x_{n+2} \dots x_{-2} d'_{L,0}, & n < 0. \end{cases} \quad (\text{A26})$$

There is a similar procedure as above to calculate the wave function coefficients of electronlike quasiparticle incident from the right. One could also get the wave functions for the leftmovers using the formulas above if the substitutions $V \rightarrow -V$, $\phi_0 \rightarrow -\phi_0$ and $\Delta_{1(2)} \rightarrow \Delta_{2(1)}$ are made.

In Eqs. (9) and (14), the density of states in the superconductors $N_\tau(E)$ is included which will give rise to discontinuities at the gap edges. This will produce numerical errors when we perform numerical calculations. Fortunately, the transmission amplitude J_τ appearing in the recurrence equation [Eq. (A15)] will only enter as a prefactor in the coefficient d , and therefore also in a , b , and c . Hence, a factor J_τ^2 can be extracted from $T^\tau(E, \theta, m)$ in Eq. (10) and Eq. (14) and combined with the density of states:

$$\begin{aligned} N_\tau(E) J_\tau^2(E) &= \frac{\theta(|E| - |\Delta_\tau|)}{|u_\tau^2 - v_\tau^2|} \left(\frac{u_\tau^2 - v_\tau^2}{u_\tau} \right)^2 \\ &= \theta(|E| - |\Delta_\tau|) (1 - A_{\tau,0}^2). \end{aligned} \quad (\text{A27})$$

The discontinuities at the gap edges are then eliminated.

Another numerical difficulty is the appearance of a number of resonances in the continued fraction expansion solution of the recurrence relation. For a particle coming in at energy E and angle θ these resonances appear if the trajectory (MAR state) hits zero energy (MGS) or the gap edges. When the integration over energy is performed, it is therefore a good idea to take special care of these points in order to faster get an accurate result.

APPENDIX B: EQUIVALENCE OF CURRENT FORMULAS

In the literature different current formulas have been used. In this Appendix we show analytically that they are all the same. In addition we have noticed that the different formulas numerically give the same results.

A very useful relation is the completeness relation

$$\sum_\nu [u_\nu(\mathbf{r}) u_\nu^*(\mathbf{r}') + v_\nu^*(\mathbf{r}) v_\nu(\mathbf{r}')] = \delta(\mathbf{r} - \mathbf{r}'), \quad (\text{B1})$$

where the sum runs over solutions to the BdG equation with positive energy.⁵⁰ We apply $\nabla_{\mathbf{r}'}$ and take the imaginary part:

$$\sum_\nu \text{Im} \{ v_\nu \nabla v_\nu^* \} = - \sum_\nu \text{Im} \{ u_\nu^* \nabla u_\nu \}. \quad (\text{B2})$$

From now on we let the sum over states (here ν) run over k -vectors, since we in this paper discuss plane wave solutions.

Next, we have the following symmetry between solutions to the BdG equation with positive and negative energies

$$\begin{aligned} u_k(E) &= -v_{-k}^*(-E) \\ v_k(E) &= u_{-k}^*(-E), \end{aligned} \quad (\text{B3})$$

where the left hand side is a solution describing an electron-like quasiparticle with energy E , and the right hand side is a solution describing a hole-like quasiparticle with energy $-E$. Both particles have positive group velocities. We can use Eq. (B3) in Eq. (B2) to get the same type of completeness also for negative energies.

The current formula can be written in the excitation picture⁴² (positive energies only) as

$$\begin{aligned} j &= \frac{e\hbar}{m} \sum_\sigma \sum_k \text{Im} \{ u_{k\sigma}^* \nabla u_{k\sigma} - v_{k\sigma} \nabla v_{k\sigma}^* \} f(E_{k\sigma}) \\ &+ \frac{e\hbar}{m} \sum_\sigma \sum_k \text{Im} \{ v_{k\sigma} \nabla v_{k\sigma}^* \}, \end{aligned} \quad (\text{B4})$$

where $\sigma = \uparrow, \downarrow$ labels spin up and spin down, see Fig. 11(a). Since in this paper a spin independent problem is featured, the spin sum just produces a factor of two. One of the terms (say $\sigma = \downarrow$) in the spin sum can be mapped into negative energies using Eq. (B3) and the relation $f(-E) = 1 - f(E)$. After this mapping to negative energy states the spin sum transforms into a summation over branches of negative ($\beta = -$) and positive ($\beta = +$) energies (sometimes denoted the semiconductor picture), see Fig. 11(b). As a result the current formula after these modifications is

$$\begin{aligned} j &= \frac{e\hbar}{m} \sum_\beta \sum_k \text{Im} \{ u_{k\beta}^* \nabla u_{k\beta} - v_{k\beta} \nabla v_{k\beta}^* \} f(E_{k\beta}) \\ &+ \frac{e\hbar}{m} \sum_\beta \sum_k \text{Im} \{ v_{k\beta} \nabla v_{k\beta}^* \}. \end{aligned} \quad (\text{B5})$$

We now study the term in Eq. (B5) without the Fermi-factor. We write out the sum over β :

$$\begin{aligned} &\sum_\beta \sum_k \text{Im} \{ v_{k\beta} \nabla v_{k\beta}^* \} \\ &= \sum_k [\text{Im} \{ v_{k+} \nabla v_{k+}^* \} - \text{Im} \{ u_{k-}^* \nabla u_{k-} \}] \\ &= \sum_k [\text{Im} \{ v_{k+} \nabla v_{k+}^* \} - \text{Im} \{ v_{-k,+} \nabla v_{-k,+}^* \}] = 0, \end{aligned} \quad (\text{B6})$$

where we in the first step used Eq. (B2) (in the negative energy branch term) and in the second step used

Eq. (B3). We therefore have the following current formula in the semiconductor picture:

$$j = \frac{e\hbar}{m} \sum_{\beta} \sum_k \text{Im} \{ u_{k\beta}^* \nabla u_{k\beta} + v_{k\beta}^* \nabla v_{k\beta} \} f(E_{k\beta}). \quad (\text{B7})$$

We may now turn the sum over hole-like quasiparticles into a sum over electron-like quasiparticles by using the symmetry in Eq. (B3) once again. The current formula will then be

$$j = \frac{e\hbar}{m} \sum_{\beta} \sum_{k=k^e} \text{Im} \{ u_{k\beta}^* \nabla u_{k\beta} + v_{k\beta}^* \nabla v_{k\beta} \} \times [2f_{FD}(E_{k\beta}) - 1], \quad (\text{B8})$$

which is the one written down in Eq. (4). The states included in Eq. (B8) is shown in Fig. 11(c).

In conclusion, we can use the completeness relation [Eq. (B2)] and the symmetry of the BdG equation [Eq. (B3)] to rewrite the formula for the current into different forms. Which form to use is a matter of convenience as long as one sums over the right set of scattering states. For instance in Refs. 13, 44, and 46 Eq. (B5) was used; on the other hand, in this paper and in Ref. 17 Eq. (B8) has been used.

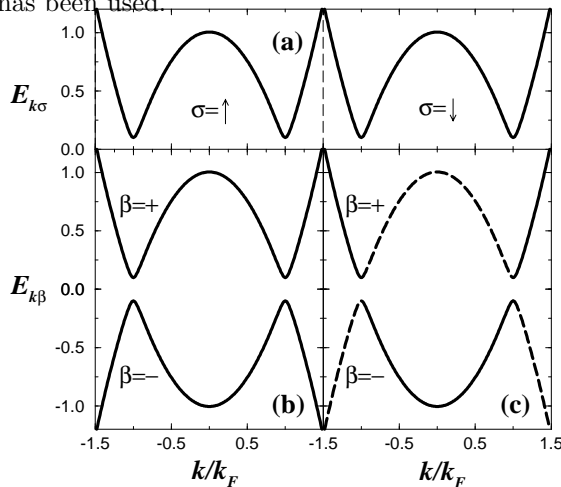


FIG. 11. Here we show the different sets of states to sum over for the different current formulas. In (a) we show the two branches with positive energies (labeled by a spin index σ) included in Eq. (B4). In (b) we show the negative ($\beta = -$) and the positive ($\beta = +$) branches included in Eq. (B7). In (c) we show the states included in Eq. (B8): only the electron-like particles are included (the solid line), while the hole-like particles are excluded (the dashed line).

APPENDIX C: SOME REMARKS ON THE CURRENT

1. Derivation of the symmetry $I(-V) = -I(V)$

In this subsection we show the relation $I(-V) = -I(V)$ for both perpendicular and parallel current density.

Letting $V \rightarrow -V$ and $E \rightarrow -E$ we see from Eq. (A3) that the Andreev reflection amplitude $A_n \rightarrow -A_n^*$. Studying Eq. (A16), this gives

$$\begin{aligned} \alpha_n &\rightarrow \alpha_n^*, \\ \beta_n &\rightarrow \beta_n^*, \\ \gamma_n &\rightarrow \gamma_n^*, \end{aligned} \quad (\text{C1})$$

implying that Eq. (A15) determining d_n changes to

$$\alpha_n^* d_{n+2} + \beta_n^* d_n + \gamma_n^* d_{n-2} = rJ(E)\delta_{n,0}. \quad (\text{C2})$$

After complex conjugation and multiplication of the factor r/r^* , we have

$$(\alpha_n d_{n+2}^* + \beta_n d_n^* + \gamma_n d_{n-2}^*) \frac{r}{r^*} = rJ(E)\delta_{n,0}. \quad (\text{C3})$$

If we compare this recurrence equation to the one in Eq. (A15), we see that

$$d_n \rightarrow d_n^* r/r^*. \quad (\text{C4})$$

Using Eq. (C4) in Eqs. (A8) and (A17), we get

$$a_n \rightarrow a_n^*, \quad (\text{C5})$$

$$b_n \rightarrow -b_n^*, \quad (\text{C6})$$

$$c_n \rightarrow -c_n^* r/r^*, \quad (\text{C7})$$

which implies [from Eq. (10)] that

$$T_x^T(E, \theta, m) \rightarrow [T_x^T(E, \theta, m)]^*. \quad (\text{C8})$$

A minus sign is extracted when we let $E \rightarrow -E$ in Eq. (9) since

$$\tanh(-E/2k_B T) \rightarrow -\tanh(-E/2k_B T). \quad (\text{C9})$$

Taking Eq. (C8) and Eq. (C9) into account we get from Eq. (9)

$$A_{x,0} \rightarrow -A_{x,0}. \quad (\text{C10})$$

Therefore, one finally finds

$$I_{x,0}(-V) = -I_{x,0}(V). \quad (\text{C11})$$

The same kind of reasoning as above for the perpendicular case is used to put the transformations Eqs. (C4)-(C7) and (C9) into the corresponding equations for $j_{y,0}$. Therefore, we also have

$$j_{y,0}(-V) = -j_{y,0}(V). \quad (\text{C12})$$

2. Disappearance of ac components

Here we set out to show analytically how the ac components disappear for some orientations of the superconducting order parameters.¹⁷ The argument presented here is not Z -dependent: it is true for any barrier strength.

The keypoint is to compare current contributions associated with injection angles $\pm\theta$ and see how they add up. We can separate the integrand which we integrate over the angles $\theta \in [-\pi/2, \pi/2]$ into two functions: first a trigonometric function and second a complicated function depending on the gaps. The trigonometric function is $\cos\theta$ (even in θ) for the x current and $\sin\theta$ (odd in θ) for the y current. We will show that the second function is odd or even in θ depending on the orientation of the superconductors. The combination of the two functions will therefore be odd in some cases and therefore integrate to zero.

Case 1: $d_0|d_0$ junction. In this case the gaps are symmetric in θ on both the left and the right side, implying that the second function is even in θ . Taking the trigonometric functions into account, the x current therefore contains all components m while the y current is zero for all m .

Case 2: $d_0|d_{\pi/4}$ junction. This case is shown in Fig. 2. The gap on the right side is oriented so that the negative lobe appears for negative angles: $\Delta_2(-\theta) = -\Delta_2(\theta) = \Delta_2(\theta) \exp(i\pi)$. This extra phase π for the negative angles can be given to ϕ_0 . As noted in Appendix A, the phase difference over the junction ϕ_0 is factored out in the beginning of the calculation, but it reappears in the phase Ω_m in the final expression for the current, see Eq. (11). We therefore have

$$\Omega_m(-\theta) = \Omega_m(\theta) + m\pi. \quad (\text{C13})$$

In addition, we have (taking also the trigonometric function into account)

$$\begin{cases} A_{x,m}(-\theta) = A_{x,m}(\theta) \\ B_{x,m}(-\theta) = B_{x,m}(\theta) \\ A_{y,m}(-\theta) = -A_{y,m}(\theta) \\ B_{y,m}(-\theta) = -B_{y,m}(\theta) \end{cases} \Rightarrow \begin{cases} C_{x,m}(-\theta) = C_{x,m}(\theta) \\ \alpha_{x,m}(-\theta) = \alpha_{x,m}(\theta) \\ C_{y,m}(-\theta) = -C_{y,m}(\theta) \\ \alpha_{y,m}(-\theta) = \alpha_{y,m}(\theta) \end{cases} \quad (\text{C14})$$

Using Eq. (C13) and Eq. (C14), we can rewrite the x current

$$\frac{I_x}{\sigma_0} = \sum_m C_{x,m}(\theta > 0) (1 + e^{im\pi}) e^{i(\Omega_m - \alpha_{x,m})}, \quad (\text{C15})$$

and the y current

$$\frac{I_y}{\sigma_0} = \sum_m C_{y,m}(\theta > 0) (1 - e^{im\pi}) e^{i(\Omega_m - \alpha_{y,m})}, \quad (\text{C16})$$

where the functions $C_{x/y,m}(\theta > 0)$ contains an integration over positive angles only. It is clear from Eq. (C15)

[Eq. (C16)] that the odd (even) components of the x (y) current will be zero for this orientation. Note that the $m = 0$ component of the y current is also zero.

Case 3: $d_{\pi/4}|d_{\pi/4}$ junction. Here we have an extra phase π on both the left and the right side for negative angles. This means that we have no effective extra phase that we can factor out together with ϕ_0 . Instead we see in Eq. (A3) that the Andreev reflection amplitudes are $A_{1/2}(-\theta) = -A_{1/2}(\theta) = A_{1/2}(\theta) \exp(i\pi)$. Studying the equations in Appendix A, only combinations of two A multiplying each other appear. Thus the extra phases π cancel. Taking also the trigonometric function into account, the integrand will therefore be even (odd) for all m components of the x (y) current in the same way as for the $d_0|d_0$ junction.

For orientations in between $\alpha_{1/2} = 0$ and $\alpha_{1/2} = \pi/4$, the cancellation effects will not be perfect and all components m are non-zero for both the x and y currents.

APPENDIX D: ANALYTIC EXPRESSIONS FOR LARGE AND SMALL VOLTAGES

1. Large voltage in the ballistic limit

In the large voltage limit ($eV \gg \Delta_0$) we only need to consider one Andreev reflection. This means that only coefficients a_n , b_n , c_n , and d_n with indices $n = 0$ and $n = \pm 2$ have to be taken into account.

In the ballistic limit ($Z = 0$), the surviving coefficients from an electron-like quasiparticle injected from the left superconductor at energy E and angle θ will be a_0^\rightarrow (the injected electron) and b_2^\rightarrow (the hole created from Andreev reflection at the right superconductor). As outlined in Ref. 46 we can then perform the integration over energy analytically in the limit $eV \rightarrow \infty$ and get the following expressions for the currents

$$\begin{aligned} \frac{I_{x,0}(V)}{\sigma_0} &= \frac{eV}{\Delta_0} + \frac{2}{3} \int_{-\pi/2}^{\pi/2} d\theta \cos\theta \left[\frac{|\Delta_1(\theta)|}{\Delta_0} + \frac{|\Delta_2(\theta)|}{\Delta_0} \right] \\ &= \frac{eV}{\Delta_0} + I_{\text{excess}}, \\ \frac{j_{y,0}}{(\sigma_0/L_y)} &= \frac{2}{3} \int_{-\pi/2}^{\pi/2} d\theta \sin\theta \left[\frac{|\Delta_1(\theta)|}{\Delta_0} + \frac{|\Delta_2(\theta)|}{\Delta_0} \right], \quad (\text{D1}) \end{aligned}$$

valid for large voltages. Note that both the excess current and the surface current is independent of voltage when $eV \gg \Delta_0$.

2. Small voltage in the ballistic limit

In the ballistic case there is a nonzero current contribution in the small-voltage limit for both the perpendicular (x) and parallel (y) direction. For the ballistic one-channel SNS junction with different s -wave gaps one

has previously derived that the perpendicular current is proportional to the smallest of the gaps.⁴⁶ Generalizing this result to our case we have for the current in the x -direction

$$\frac{I_x}{\sigma_0} = \int_{-\pi/2}^{\pi/2} d\theta \cos \theta \min\left(\frac{|\Delta_1(\theta)|}{\Delta_0}, \frac{|\Delta_2(\theta)|}{\Delta_0}\right). \quad (\text{D2})$$

In the same way we find for the parallel current density in the normal region that

$$\frac{j_y}{(\sigma_0/L_y)} = \int_{-\pi/2}^{\pi/2} d\theta \sin \theta \min\left(\frac{|\Delta_1(\theta)|}{\Delta_0}, \frac{|\Delta_2(\theta)|}{\Delta_0}\right). \quad (\text{D3})$$

* Present address: AXE Research and Development, Ericsson, Box 1505, S-125 25 Älvsjö, Sweden.

- ¹ D. A. Wollman, D. J. van Harlingen, W. C. Lee, D. M. Ginsberg, and A. J. Leggett, Phys. Rev. Lett. **71**, 2134 (1993).
- ² D. J. Van Harlingen, Rev. Mod. Phys. **67**, 515 (1995) and references therein.
- ³ K. A. Kouznetsov, A. G. Sun, B. Chen, A. S. Katz, S. R. Bahcall, J. Clark, R. C. Dynes, D. A. Gajewski, S. H. Han, M. B. Maple, J. Giapintzakis, J.-T. Kim, and D. M. Ginsberg, Phys. Rev. Lett. **79**, 3050 (1997).
- ⁴ C. C. Tsuei, J. R. Kirtley, Z. F. Ren, J. H. Wang, H. Raffy, and Z. Z. Li, Nature **387**, 481 (1997).
- ⁵ J. Geerk, X. X. Xi, and G. Linker, Z. Phys. B **73**, 329 (1988).
- ⁶ M. Covington, M. Aprili, E. Paraoanu, L. H. Greene, F. Xu, J. Zhu, and C. A. Mirkin, Phys. Rev. Lett. **79**, 277 (1997).
- ⁷ S. Sinha and K.-W Ng, Phys. Rev. Lett. **80**, 1296 (1998).
- ⁸ L. Alff, H. Takashima, S. Kashiwaya, N. Tereda, H. Ihara, Y. Tanaka, M. Koyanagi, and K. Kajimura, Phys. Rev. B **55**, R14757 (1997).
- ⁹ L. Alff, A. Beck, R. Gross, A. Marx, S. Kleefisch, Th. Bauch, H. Sato, M. Naito, and G. Koren, to appear in Phys. Rev. B [cond-mat/9805162].
- ¹⁰ L. Alff, S. Kleefisch, U. Schoop, M. Zittartz, T. Kemen, T. Bauch, A. Marx, and R. Gross, to appear in Eur. Phys. J. B [cond-mat/9806150].
- ¹¹ C.-R. Hu, Phys. Rev. Lett. **72**, 1526 (1994).
- ¹² Y. Tanaka and S. Kashiwaya, Phys. Rev. Lett. **74**, 3451 (1995).
- ¹³ M. Hurd, Phys. Rev. B **55**, R11993 (1997).
- ¹⁴ Yu. S. Barash and A. A. Svidzinsky, Czech. J. Phys. **46**, 1013 (1996).
- ¹⁵ Yu. S. Barash and A. A. Svidzinsky, in *Quasiclassical Theory of Superconductivity in Strongly Correlated Systems*, edited by D. Rainer and J. A. Sauls (Springer-Verlag, 1997).
- ¹⁶ G. Wendin, Appl. Supercon. **5**, in press.
- ¹⁷ T. Löfwander, G. Johansson, M. Hurd, and G. Wendin, Phys. Rev. B **57**, R3225 (1998).
- ¹⁸ E. A. Early, A. F. Clark, and K. Char, Appl. Phys. Lett. **62**, 3357 (1993).
- ¹⁹ S. K. Yip, O. F. de Alcantara Bonfim, and P. Kumar, Phys. Rev. B **41**, 11214 (1990).
- ²⁰ S. K. Yip, J. Low Temp. Phys. **91**, 203 (1993).
- ²¹ Y. Tanaka and S. Kashiwaya, Phys. Rev. B **56**, 892 (1997).
- ²² A. M. Zagoskin, J. Phys.: Condens. Matter **9**, L419 (1997).
- ²³ M. Sigrist, K. Kuboki, P. A. Lee, A. J. Millis, and T. M. Rice, Phys. Rev. B **53**, 2835 (1996).
- ²⁴ W. Belzig, C. Bruder, and M. Sigrist, Phys. Rev. Lett. **80**, 4285 (1998).
- ²⁵ D. L. Feder, A. Beardsall, A. J. Berlinsky, and C. Kallin, Phys. Rev. B **56**, R5751 (1997).
- ²⁶ M. Matsumoto and H. Shiba, J. Phys. Soc. Jpn. **64**, 3384 (1995); **64**, 4867 (1995).
- ²⁷ L. J. Buchholtz, M. Palumbo, D. Rainer, and J. A. Sauls, J. Low Temp. Phys. **101**, 1079 (1995); **101**, 1099 (1995).
- ²⁸ M. Fogelström, D. Rainer, and J. A. Sauls, Phys. Rev. Lett. **79**, 281 (1997).
- ²⁹ A. Huck, A. van Otterlo, and M. Sigrist, Phys. Rev. B **56**, 14163 (1997).
- ³⁰ M. Fogelström, and S. K. Yip, Phys. Rev. B **57**, R14060 (1998).
- ³¹ M. H. Cohen, L. M. Falicov, and J. C. Phillips, Phys. Rev. Lett. **8**, 316 (1962).
- ³² B. D. Josephson, Phys. Letters **1**, 251 (1962).
- ³³ V. Ambegokar and A. Baratoff, Phys. Rev. Lett. **10**, 593 (1963).
- ³⁴ G. E. Blonder, M. Tinkham, and T. M. Klapwijk, Phys. Rev. B **25**, 4515 (1982).
- ³⁵ C. W. J. Beenakker and H. van Houten, Phys. Rev. Lett. **66**, 3056 (1991).
- ³⁶ C. W. J. Beenakker, Phys. Rev. Lett. **67**, 3836 (1991).
- ³⁷ U. Gunsenheimer and A. D. Zaikin, Phys. Rev. B **50**, 6317 (1994).
- ³⁸ E. N. Bratus, V. S. Shumeiko, and G. Wendin, Phys. Rev. Lett. **74**, 2110 (1995).
- ³⁹ D. Averin and A. Bardas, Phys. Rev. Lett. **75**, 1831 (1995).
- ⁴⁰ V.S. Shumeiko, E.N. Bratus, and G. Wendin, Low Temp. Phys. **23**, 181 (1997).
- ⁴¹ E. N. Bratus, V. S. Shumeiko, E. V. Bezuglyi, and G. Wendin, Phys. Rev. B **55**, 12666 (1997).
- ⁴² P. G. de Gennes, *Superconductivity of Metals and Alloys* (Addison-Wesley, New York, 1989).
- ⁴³ A. F. Andreev, Sov. Phys. JETP **50**, 1228 (1964).
- ⁴⁴ M. Hurd, S. Datta, and P. F. Bagwell, Phys. Rev. B **56**, 11 232 (1997).
- ⁴⁵ C. Bruder, Phys. Rev. B **41**, 4017 (1990).
- ⁴⁶ M. Hurd, S. Datta, and P. F. Bagwell, Phys. Rev. B **54**, 6557 (1996).
- ⁴⁷ J. Bardeen, L. N. Cooper, and J. R. Schrieffer, Phys. Rev. **108**, 1175 (1957).
- ⁴⁸ M. P. Samanta and S. Datta, Phys. Rev B **57**, 10972 (1998).
- ⁴⁹ W. H. Press, S. A. Teukolsky, W. T. Vetterling, and B. P. Flannery, *Numerical Recipes in C*, Cambridge University Press, Cambridge, 1986.
- ⁵⁰ J. Bardeen, R. Kümmel, A. E. Jacobs, and L. Tewordt, Phys. Rev. **187**, 556 (1969).